Monte Carlo calculation of inter-valence-band radiation absorption in germanium. II. High-intensity absorption

1989 J. Phys.: Condens. Matter 1 9653

(http://iopscience.iop.org/0953-8984/1/48/014)

J. Phys.: Condens. Matter **1** (1989) 9653–9663. Printed in the UK

Monte Carlo calculation of inter-valence-band radiation absorption in germanium: II. High-intensity absorption

A Dargys
Institute of Semiconductor Physics, Academy of Sciences of the Lithuanian SSR, 232600 Vilnius, Lithuania, USSR

Received 30 November 1988

Abstract. The Monte Carlo method described in paper I is used to find heavy- and light-hole distribution functions and inter-valence absorption cross sections at high infrared laser intensities. At such intensities a hole is burned out in the hole distribution function and, as a result, the p-type semiconductor becomes transparent. The graphs of inter-valence absorption cross sections as a function of NH_3 and CO_2 laser electric field strength inside the semiconductor are presented for p-type germanium at two lattice temperatures, $T = 300$ and 77 K, and compared with the available experimental results. The paper also demonstrates how the Monte Carlo method can be extended to include valence band warping and non-parabolicity.

1. Introduction

In paper I (Dargys 1989) the Monte Carlo (MC) model for simulation of infrared (IR) absorption due to hole inter-valence transitions is described and used to calculate absorption cross sections at low radiation intensities. In the model the heavy- (h) and light- (l) mass valence sub-bands are treated as an ensemble of two-level systems characterised by hole wavevector components parallel k_{z0} and perpendicular $k_{\perp 0}$ to the laser electric field. The hole, due to instantaneous collisions with the phonons, is allowed to jump from one two-level system to another. If between collisions the two-level system happens to be in resonance with the radiation field, the hole interacts with the field and, as a result, absorbs or emits photons.

A separate two-level system is looked upon as a micro-ensemble of holes with equal k_{z0} and $k_{\perp 0}$. The interaction of the micro-ensemble with the field is described by open Bloch equations, which take into account such purely quantum-mechanical effects as Rabi oscillations and dephasing and, at the same time, allow particle exchange with other two-level systems. To conserve particle population between collisions on the considered two-level system, additional feeding and decay terms are included in the Bloch equations, as proposed by Breiland *et al* (1976).

Two types of solutions of the open Bloch equations, in the following referred to as the s- and t-cases, are used to simulate hole interaction with the radiation field. In the s-case it is assumed that the probability to find the hole on the upper and lower level is independent of time, and can be described by stationary solutions of the Bloch equations. In contrast, in the t-case it is assumed that the hole population on both levels oscillates with the Rabi frequency; the character of the oscillations (which in general can be

0953-8984/89/489653 + 11 $02.50

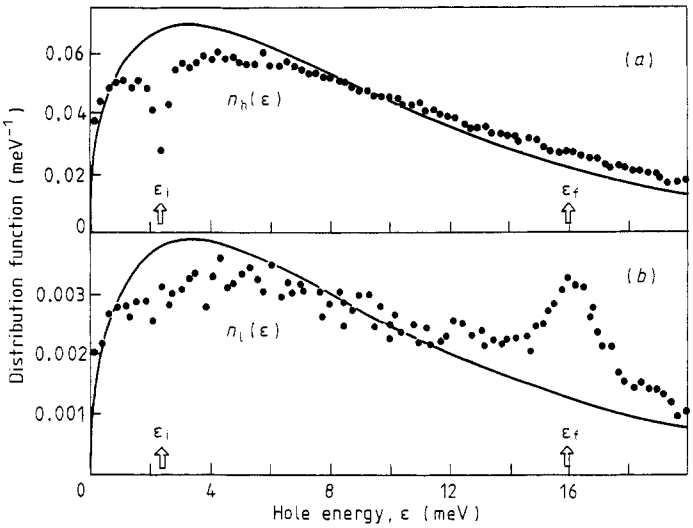

Figure 1. (*a*) Heavy- and (*b*) light-hole distribution functions in p-Ge at 77 K. Dots are MC simulations at NH_3 laser intensity $I = 13.6$ kW cm^{-2}, which corresponds to an electric field amplitude inside the semiconductor of $F_0 = 1.6$ kV cm^{-1}. Full curves show equilibrium distribution function (3). The arrows indicate the initial and final hole energies at exact resonance.

damped) is determined by the transient solution. In both cases the upper and lower level populations depend on the IR radiation intensity.

In this paper the MC method is employed to calculate the absorption cross section in p-Ge subjected to intense IR laser radiation. As demonstrated by Bishop *et al* (1976) and Keilmann (1977) at such intensities a hole is burned in the hole distribution function. This, along with the increase of induced emission, leads to a decrease in the absorption, and ensuing transparency of the semiconductor. In this paper the absorption cross section as a function of electric field amplitude inside the semiconductor has been calculated at the wavelength of NH_3 and CO_2 lasers at liquid–nitrogen and room temperatures, and compared with the available experimental data. To demonstrate the strength of the present MC method it has been extended to warped valence bands, a problem that is insurmountable by analytical methods.

Hole scattering mechanisms and probabilities used in the MC simulation are summarised in Appendix 2. The self-scattering mechanism (Rees 1969), which is so indispensable in constant field transport simulation, was omitted here as explained in Appendix 1. Constants of p-Ge used in the MC program can be found in paper I.

2. Non-linear absorption of NH_3 laser radiation

The points in figure 1 demonstrate the deformation of heavy- and light-hole distribution functions in p-Ge at lattice temperature $T = 77$ K and at the NH_3 laser electric field amplitude $F_0 = 1.6$ kV cm^{-1}. The s-case formulae have been used and approximately 10^6 collisions with phonons have been simulated. Arrows indicate the initial and final hole energies participating in optical transitions at exact resonance, when detuning $\Delta = (\omega_r - \omega)/\omega = 0$,

$$\varepsilon_i = \hbar\omega/[(m_h/m_l) - 1] \tag{1}$$

$$\varepsilon_f = \varepsilon_i + \hbar\omega \tag{2}$$

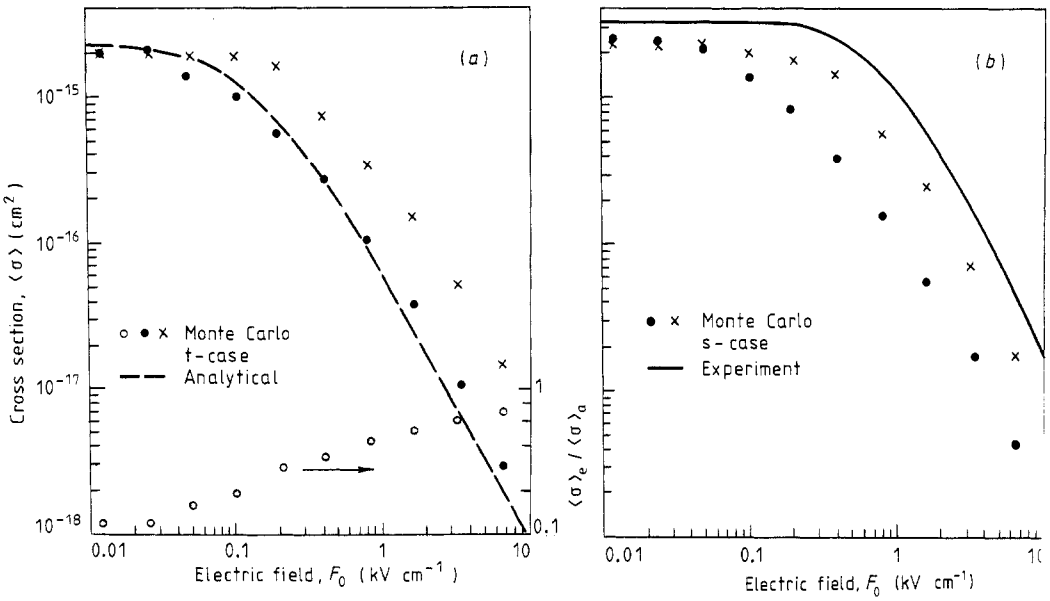

Figure 2. Inter-valence absorption cross section of p-Ge as a function of NH_3 laser electric field amplitude at $T = 77$ K. The points are MC calculations: (*a*) t-case, (*b*) s-case. Full and open circles correspond to acoustic scattering rate approximated by (A2.1), while crosses correspond to four times larger acoustic scattering rate. Open circles show the cross-section ratio. $1/\tau_2^* = 0$. The full curve represents averaged experimental results of Beregulin *et al* (1987). The broken curve is theoretical calculations by Parshin and Shabayev (1987).

where $\hbar\omega$ ($=13.63$ meV) is the energy of the NH_3 laser. A hole burned in the heavy-hole distribution function at $\varepsilon_i = 2.35$ meV and a peak in the light-hole distribution function at $\varepsilon_f = 15.98$ meV are clearly seen. For reference, the equilibrium distribution functions

$$n_{h,l}(\varepsilon) = \frac{2}{\sqrt{\pi}} \frac{m_{h,l}^{3/2}}{m_h^{3/2} + m_l^{3/2}} \frac{\sqrt{\varepsilon}}{(kT)^{3/2}} e^{-\varepsilon/kT} \tag{3}$$

are drawn using full curves. They are normalised so that $\int_0^\infty (n_h + n_l)\, d\varepsilon = 1$.

The dependence of the total absorption cross section $\langle\sigma\rangle = \langle\sigma\rangle_a - \langle\sigma\rangle_e$ on F_0 for two scattering rates with acoustic phonons are shown by full circles and crosses in figure 2(*a*) for the t-case and in figure 2(*b*) for the s-case. The ratio $\langle\sigma\rangle_e/\langle\sigma\rangle_a$, which reflects how fast emission and absorption processes equalise with the increase of F_0, are plotted using open circles. The cross sections $\langle\sigma\rangle_e$ and $\langle\sigma\rangle_a$ are associated with induced emission and pure absorption (see (I. 25) and (I.26)†).

Two mechanisms, which are responsible for the decrease of $\langle\sigma\rangle$ with electric field, could be distinguished. The first is connected with the disturbance of the detailed balance between incoming and outgoing hole fluxes in the resonance region, where $\varepsilon \simeq \varepsilon_i$; the increase of F_0 increases the outgoing flux faster than the incoming one. This process yields an overall deformation of the distribution function and is controlled by hole energy relaxation. The second mechanism is connected with the equalisation of probabilities to find the hole in h and l sub-bands at high laser intensities. The latter is directly associated with the dip in the heavy-hole distribution function in the resonance region. As can be seen from (I.8) the probability to find the hole in the h sub-band tends towards $\frac{1}{2}$ as F_0 increases. The same arguments remain true for the t-case also.

† The formulae of paper I are denoted in this way.

Because of their small number at low temperatures, optical phonons play a negligible role in the hole thermalisation dynamics. In addition, the optical phonon energy, $\varepsilon_{op} = 37.4$ meV, is larger than the hole final energy ε_f, and, as a result, optical phonon emission by holes having energies $\varepsilon \simeq \varepsilon_f$ is forbidden. A theory based on density matrix formalism for parabolic bands and acoustic scattering mechanism was developed by Parshin and Shabayev (1987). Their results are plotted in figure 2(*a*) by the broken curve.

The full curve in figure 2(*b*) represents averaged experimental results of a sample with hole concentration $p = 3 \times 10^{14}$ cm^{-3} measured by Beregulin *et al* (1987), and approximated by formula†

$$\langle\sigma\rangle = \sigma_0/[1 + (F_0/F_c)^2] \tag{4}$$

with $\sigma_0 = 3.2 \times 10^{-15}$ cm^2 and $F_c = 0.75$ kV cm^{-1}.

The effect of the dephasing time

$$t_2 = [(t_h^{-1} + t_l^{-1})/2 + t_2^{*-1}]^{-1}$$

and free flight times t_h and t_l was investigated by varying either pure dephasing time t_2^*, or acoustic scattering rate (see Appendix 2). It was found that t_2^* only slightly influences the magnitude of $\langle\sigma\rangle$. A much stronger dependence of $\langle\sigma\rangle$ on the acoustic scattering rate was observed. The full circles and crosses in figure 2 correspond to decoupled h and l sub-band free flight times $t_h = 19.7$ ps, $t_l = 7.9$ ps and $t_h = 5.5$ ps, $t_l = 2.08$ ps, respectively, in the resonance region. The larger scattering rate on acoustic phonons gives closer agreement with the experiment.

Analysis of MC results in figures 2(*a*) and 2(*b*) does not allow one to give a definite preference either to stationary (s) case formulae (see (I.8) and (I.9)) or to transient (t) case formulae (see (I.10) and (I.11*a*)), although the s-case yields slightly better agreement with the experiment.

The structure of the MC program permits inclusion of two-photon or higher-order photon absorption rather easily. Using two-photon formulae deduced by Dargys (1987), it was evaluated that at the largest investigated electric field in figure 2 the two-photon contribution to the total absorption cross section does not exceed a few per cent.

3. Non-linear absorption of CO_2 laser radiation

The points in figures 3 and 4 demonstrate the dependence of the absorption cross section on F_0 found by the MC method at CO_2 laser wavelengths. Experimental results are represented by full curves. Measurements at 77 K by Beregulin *et al* (1982) are approximated with formula (4) and parameters $\sigma_0 = 3.8 \times 10^{-16}$ cm^2, $F_c = 10$ kV cm^{-1}. At 300 K, according to Phipps and Thomas (1977), the experimental results are described better with

$$\langle\sigma\rangle = \sigma_0/[1 + (F_0/F_c)^2]^{1/2} \tag{5}$$

with $\sigma_0 = 7 \times 10^{-16}$ cm^2 and $F_c = 24.5$ kV cm^{-1}. It is evident that at both temperatures the MC calculations with s-case formulae (crosses) are closer to the experimental curves. This remains true even if the laser energy is somewhat varied.

Light- and heavy-hole distribution functions for CO_2 laser electric field 16 kV cm^{-1} (this corresponds to $I = 1.36$ MW cm^{-2}) and $T = 77$ K are plotted in figure 5. Similarly

† Beregulin *et al* recommend the critical field value $F_c = 1.23$ kV cm^{-1}. With a special computer program, which takes into account multiple reflections in non-linear media, I found that the experimental results of Beregulin *et al* (1987) presented in figure 1 of their paper are better described by $F_c = 0.75$ kV cm^{-1}.

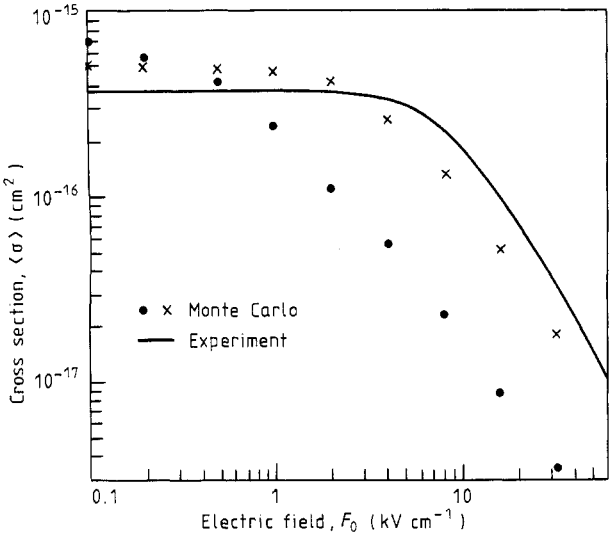

Figure 3. Inter-valence absorption cross section of p-Ge as a function of CO_2 laser electric field amplitude at $T = 77$ K. Crosses are MC calculations with s-case formulae and photon energy $\hbar\omega = 117$ meV. Dots are MC calculations with t-case formulae and $\hbar\omega = 100$ meV. $1/\tau_2^* = 0$. The full curve represents averaged experimental results of Beregulin *et al* (1982), $\hbar\omega = 117$ meV.

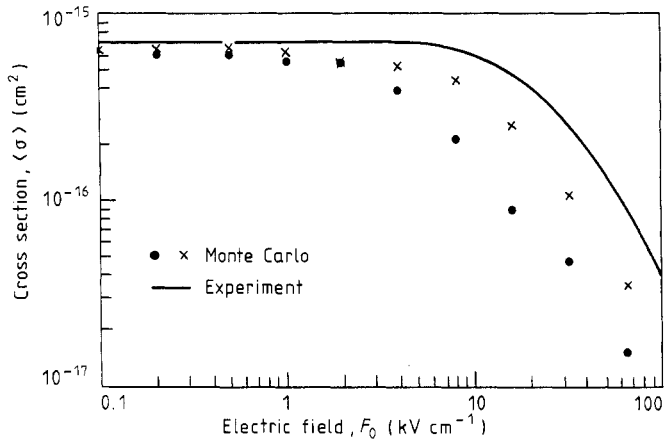

Figure 4. Inter-valence absorption cross section of p-Ge as a function of CO_2 laser electric field amplitude at $T = 300$ K. Crosses are MC calculations with s-case formulae and $\hbar\omega = 117$ meV. Dots are MC calculations with t-case formulae and $\hbar\omega = 100$ meV. $1/\tau_2^* = 0$. The full curve represents averaged experimental results of Phipps and Thomas (1977), $\hbar\omega = 117$ meV.

to figure 1, a hole is burnt in the heavy-hole distribution function at initial energy $\varepsilon_i = 20.17$ meV, and a peak appears in the light-hole distribution function at final energy $\varepsilon_f = \varepsilon_i + \hbar\omega = 137.17$ meV. Now, the decoupled sub-band free flight times in the resonance region are $t_h = 7.2$ ps and $t_l = 0.3$ ps. Since at large energies optical phonon emission dominates, the hole after excitation emits a cascade of optical phonons and, as a result, peaks (indicated by small arrows in figure 5) appear. The peaks are washed out due to scattering by acoustic phonons.

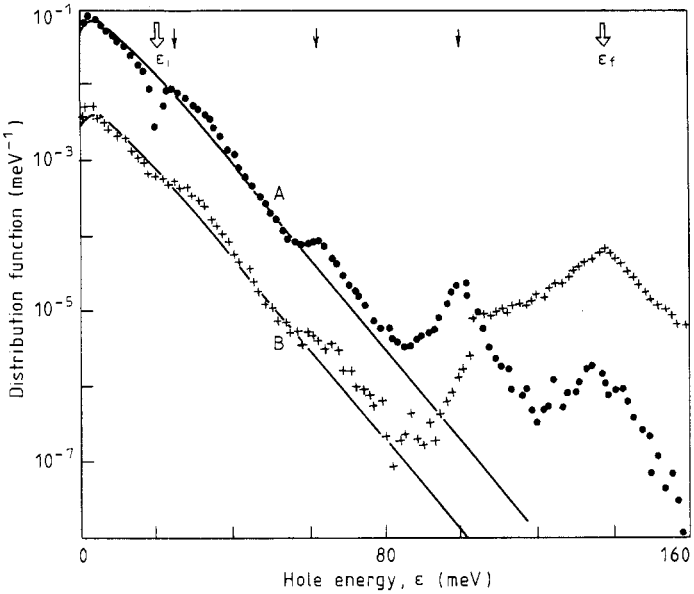

Figure 5. (A) Heavy- and (B) light-hole distribution functions in p-Ge at 77 K under CO_2 laser excitation with $F_0 = 16$ kV cm^{-1} and $\hbar\omega = 117$ meV. For reference, equilibrium distribution functions are shown by full curves. Large arrows indicate the initial and final hole energies at exact resonance, while small arrows indicate hole energies after cascade emission of one, two and three optical phonons. s-case. $1/\tau_2^* = 0$.

At hole energies $\varepsilon > \varepsilon_{op}$ the emission of optical phonons in p-Ge is rather strong; therefore, one expects an increase of the absorption cross section when the laser energy is a multiple of the optical phonon energy: $\hbar\omega = n\varepsilon_{op}$, $n = 1, 2, 3, \ldots$. That this is true can be seen in figure 6, where apart from the absorption cross section the average hole energy $\langle\varepsilon\rangle = \langle\varepsilon_h\rangle + \langle\varepsilon_l\rangle$ (see (I.28)) is also plotted. Figure 6 clearly demonstrates that both $\langle\varepsilon\rangle$ and $\langle\sigma\rangle$ oscillate with period equal to the optical phonon energy, and that the average hole energy may be lower than the thermal equilibrium one. The cooling of holes is mainly associated with hole accumulation in the low-energy region, $\varepsilon < 3kT/2$, where the energy exchange rate with the lattice is very slow, and the dip in the hole distribution function at $3kT/2 < \varepsilon < \varepsilon_{op}$.

4. Inclusion of valence band warping

In this section, absorption within warped valence sub-bands is calculated using t-case formulae. To do this one must know how Rabi oscillations should be modified for warped bands, a very difficult and as yet unsolved problem. In the following we shall assume that the expressions (I.11*a*) and (I.11*b*), which describe the dependence of l sub-band population on time, remain valid for warped bands as well, but now the Rabi frequency Ω is replaced by anisotropic Rabi frequency Ω_a. Generalisation to warped bands is accomplished with the help of the formulae obtained within first-order perturbation theory.

First of all, it will be noticed that within first-order perturbation theory the tunnelling probability (or probability to find the hole at the moment t in l sub-band) for spherical valence bands can be expressed through the Rabi frequency:

$$r_l = \tfrac{1}{2}\pi\Omega^2\omega_\tau t. \tag{6}$$

Equation (6) can be deduced from (I.1) after integration over detuning Δ, and keeping

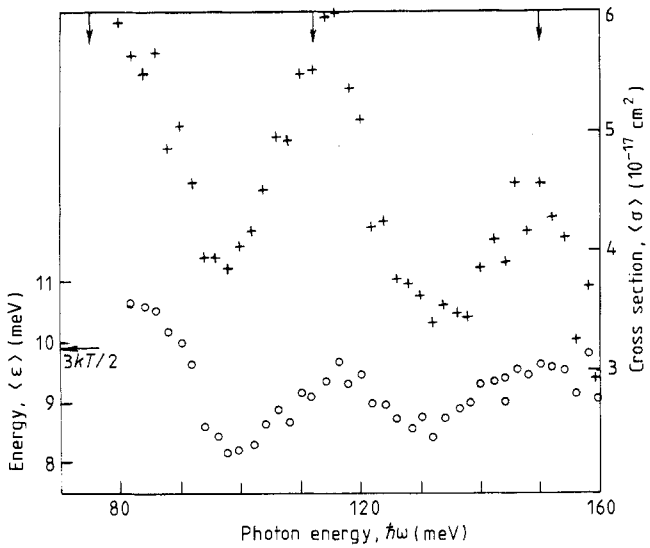

Figure 6. Variation of absorption cross section (crosses) and average hole energy (circles) with laser energy in p-Ge, at $T = 77$ K and $F_0 = 16$ kV cm^{-1}. Arrows indicate laser energies when the condition $\hbar\omega = n\varepsilon_{op}$ ($n = 2$, 3 and 4) is satisfied. s-case. $1/\tau_2^* = 0$. A single point corresponds approximately to 1.3×10^5 collisions with the phonons. The scatter of points indicates the accuracy of the present MC method.

in mind that in first-order perturbation theory $1 \ll \omega t \ll 2\pi/\Omega$ and $r_1 \ll 1$ (Dargys 1987). Secondly, the most general expression, for r_1, which takes into account valence band warping and the finite value of the phonon wavevector $\boldsymbol{\kappa}$, was obtained by Normantas (1982). We shall neglect the phonon wavevector, $\boldsymbol{\kappa} = 0$. Then the expression of Normantas for r_1 can be rewritten in the form (6), but with Ω^2 replaced by

$$\Omega_a^2 = \tfrac{3}{4}\Theta^2\Phi^2 \tag{7}$$

where Θ is the tunnelling constant for spherical bands (I.3) and Φ^2 is the anisotropy factor, which takes into account the dependence of the Rabi frequency on hole wavevector and laser electric field orientation with respect to the crystallographic axis:

$$\Phi^2 = \frac{16}{3}\frac{1}{Q_3^2}\left(Q_1 - \frac{Q_2^2}{Q_3}\right) \tag{8}$$

$$Q_1 = 3 + (\boldsymbol{e}\cdot\boldsymbol{q})^2 + 3\xi[(e_1q_2 + e_2q_1)^2 + (e_1q_3 + e_3q_1)^2 + (e_2q_3 + e_3q_2)^2] \tag{9}$$

$$Q_2 = 4(\boldsymbol{e}\cdot\boldsymbol{q}) + 6\xi[q_1q_2(e_1q_2 + e_2q_1) + q_1q_2(e_1q_3 + e_3q_1) + q_2q_3(e_2q_3 + e_3q_2)] \tag{10}$$

$$Q_3 = 4 + 12\xi(q_1^2q_2^2 + q_1^2q_3^2 + q_2^2q_3^2). \tag{11}$$

Here e_i and q_i are projections of photon polarisation and unit hole wavevector onto the crystallographic axis: $\boldsymbol{e} = \boldsymbol{F}_0/|\boldsymbol{F}_0| = (e_1, e_2, e_3)$, $\boldsymbol{q} = \boldsymbol{k}/|\boldsymbol{k}| = (q_1, q_2, q_3)$. Also, ξ is the warping constant, $\xi = (\gamma_3/\gamma_2)^2 - 1$, and γ_1, γ_2, γ_3 are valence band parameters. For spherical bands, when $\gamma_2 = \gamma_3 \equiv \gamma$, (8)–(11) reduce to $Q_1 = 3 + \cos^2\theta$, $Q_2 = 4\cos\theta$, $Q_3 = 4$ and $\Phi^2 = \sin^2\theta$, where θ is the angle between hole wavevector $\boldsymbol{k}$ and electric field $\boldsymbol{F}_0$.

The full curves in figure 7 illustrate the change of Φ^2 with azimuthal φ and polar θ_p angles that the hole wavevector makes with the crystallographic axis. The valence band

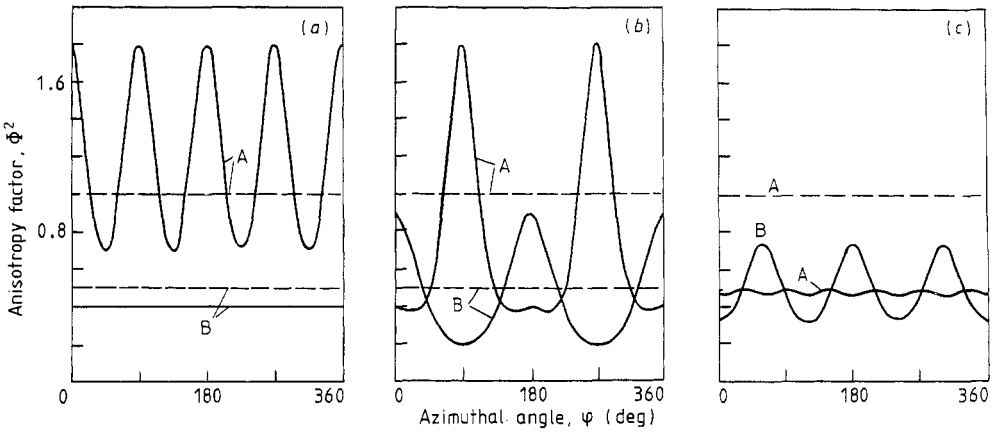

Figure 7. The anisotropy factor Φ^2 as a function of azimuthal φ and polar θ_p angles ($1 - \theta_p = \pi/4$, $2 - \theta_p = \pi/2$) for three directions of polarisation vector: (*a*) $e\|\langle 001\rangle$; (*b*) $e\|\langle 011\rangle$; (*c*) $e\|\langle 111\rangle$. All angles are read with respect to the crystallographic axis. The broken horizontal lines correspond to spherical bands.

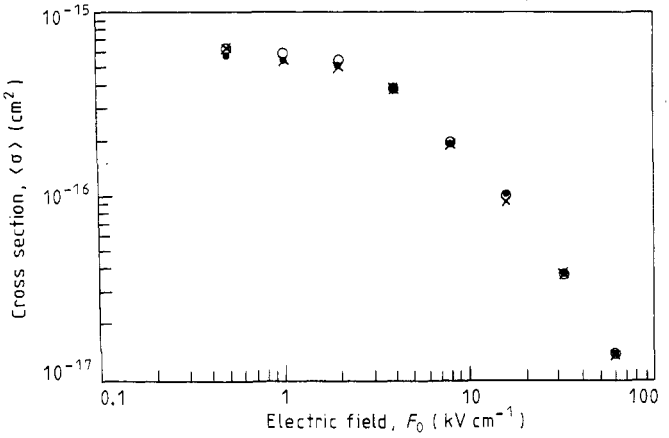

Figure 8. The dependence of absorption cross section on the electric field parallel to three main crystallographic directions: crosses, $e\|\langle 001\rangle$; dots, $e\|\langle 011\rangle$; open circles, $e\|\langle 111\rangle$. T = 300 K, $\hbar\omega$ = 100 meV, t-case, CO_2 laser.

parameters typical of p-Ge were used: $\gamma_1 = 13.35$, $\gamma_2 = 4.25$, $\gamma_3 = 5.69$. For reference, the values of Φ^2 when band warping is neglected are shown by broken horizonal lines. From figure 7 it may be concluded that the inter-valence tunnelling probability depends rather strongly on the hole wavevector direction and can vary up to five times.

In figure 8 the absorption cross section is plotted for laser electric field parallel to three main crystallographic directions. In the MC calculation the resonance energy ω_r, which appears in Δ and Θ, was replaced by an expression characteristic of anisotropic bands, i.e.

$$\hbar\omega_r = 2\frac{\hbar^2 k^2}{2m_0}\gamma_2\sqrt{Q_3}. \tag{12}$$

At high fields, within the uncertainty of the calculation, no anisotropy can be seen in the absorption cross section in figure 8. This agrees with the experimental results of Phipps and Thomas (1977) on non-linear absorption in p-Ge.

In a similar manner the effect of non-parabolicity on inter-valence transitions, investigated within first-order perturbation theory by Kane (1956), can be incorporated in the MC program. The inclusion of non-parabolicity will reduce the Rabi frequency and, consequently, will increase the absorption cross section at large photon energies.

5. Summary and conclusions

In this paper, the MC method to simulate inter-valence absorption at low and high laser intensities has been worked out. To this end, first of all, the valence band states in the presence of a laser field have been reduced to an ensemble of two-level systems. The main argument that lies behind such reduction is that in the absence of scattering the hole inter-valence dynamics in the laser field is described by exactly the same equation as a simple two-level system. This may not be evident at first sight since, in fact, in the laser field the hole, apart from inter-valence transitions, simultaneously performs harmonic motion in $\boldsymbol{k}$-space.

Secondly, the dynamics of the hole on the particular two-level system is treated as a two-step process: (i) the absorption or induced emission of a quantum of radiation by the hole during its free flight time and (ii) instantaneous hole transition to another two-level system due to hole interaction with the lattice vibrations. To take into account quantum-mechanical effects, such as Rabi oscillations and dephasing, open Bloch equations, which take into account particle exchange between different two-level systems, are employed. Two types of solutions are considered. In the t-case the hole dynamics between collisions is simulated by a transient solution, while in the s-case this is done by the stationary solution of the open Bloch equation. No preference can be given to either case at weak intensities and at high NH_3 laser intensities. However, s-case formulae were found to describe the experimental results on the non-linear absorption at high CO_2 laser intensities better.

The hole scattering by phonons at large detunings, when the two-level system is off-resonance, was treated in the standard way. At small detunings, when levels are coupled by the laser field, the resulting hole free flight time was calculated as a combination of decoupled-band free flight times, which at large laser energies may differ by an order of magnitude. In general, it has been found that the non-linear absorption cross section is roughly in inverse proportion to the free flight time in the high-field region. The contribution of pure dephasing to the increase of absorption cross section was found to be negligible; therefore, all calculations were performed with zero dephasing rate, $1/\tau_2^* = 0$.

In the MC simulation only lattice scattering was taken into account, although there are no obstacles to including impurity scattering and electron–electron scattering, and thus to extend calculations to large free-hole concentrations. Also, the multiphoton effects can easily be incorporated into the MC program. The inclusion of two-photon absorption has shown that within the investigated field range its contribution is small and can be neglected.

Nearly all calculations were performed for spherical and parabolic energy bands. At the end it was demonstrated how inter-valence transition matrix elements obtained by first-order perturbation theory could be used at high laser intensities. In particular, the inclusion of valence band warping into the MC program, in agreement with experimental results, gave no anisotropy associated with the laser polarisation.

Appendix 1. Oscillating component of the hole wavevector

Under the action of the laser electric field $F_0 \cos \omega t$, the hole wavevector component parallel to F_0 changes according to the law

$$k_z(t) = k_{z0} + \frac{eF_0}{\hbar\omega} \sin \omega t. \tag{A1.1}$$

In MC calculations the oscillatory part of $k_z(t)$ was neglected. This has allowed us to dispense with the fictitious 'self-scattering' mechanism and to find scattering probabilities immediately after the final wavevector is known. The requirement that in the expression $\hbar^2 k_z^2(t)/2m^*$ the amplitude of the energy $eF\hbar k_{z0}/m^*\omega$, which is oscillating with the laser frequency, is small, and the assumption that $\hbar^2 k_{z0}^2/2m^*$ is of the order of $3kT/2$, yield the following condition for the amplitude of the electric field:

$$F_0 < (\omega/2e)[3kTm^*]^{1/2}. \tag{A1.2}$$

At $T = 77$ K and $m^* = 0.05$ (A1.2) gives $F_0 < 7.8$ kV cm^{-1} for NH_3 laser, and $F_0 < 67$ kV cm^{-1} for CO_2 laser.

Appendix 2. Scattering mechanisms

In the program only the scattering on lattice vibrations is taken into account. The decoupled h and l sub-band scattering rates, t_h^{-1} and t_l^{-1}, are assumed to be independent of laser intensity. The validity of this assumption is indirectly confirmed by experiments on n-Ge up to CO_2 laser intensities 20 MW cm^{-2} (Yuen *et al* 1980), where the absorption coefficient has been found to be independent of the laser intensity.

It is convenient to introduce the symbol P_{ij}^{kl} for scattering rates per unit time of the hole with energy ε. For example, P_{hl}^{ae} indicates that the scattering rate is associated with the hole transition from h to l sub-band due to acoustic (a) phonon emission (e).

Acoustic phonon scattering rates

These were approximated by empirical formulae. For this purpose the graphs calculated by Reggiani *et al* (1977) were used.

Intra-sub-band scattering probabilities:

$$P_{hh}^{aa} = 0.0168\varepsilon^{0.4166} \qquad P_{hh}^{ae} = 0.0104\varepsilon^{0.626} \qquad \text{at } T = 77 \text{ K} \tag{A2.1}$$

$$P_{hh}^{aa} = P_{hh}^{ae} = 0.05\sqrt{\varepsilon} \qquad \text{at } T = 300 \text{ K} \tag{A2.2}$$

$$P_{ll}^{aa} = (m_l/m_h)^{3/2} P_{hh}^{aa} \qquad P_{ll}^{ae} = (m_l/m_h)^{3/2} P_{hh}^{ae}. \tag{A2.3}$$

Inter-sub-band scattering probabilities:

$$P_{hl}^{aa} = P_{ll}^{aa} \qquad P_{hl}^{ae} = P_{ll}^{ae} \qquad P_{lh}^{aa} = P_{hh}^{aa} \qquad P_{lh}^{ae} = P_{hh}^{ae}. \tag{A2.4}$$

In (A2.1)–(A2.4) the hole energy is measured in meV and P_{ij}^{kl} in ps^{-1}.

Optical phonon scattering rates

Intra-sub-band scattering probabilities:

$$P_{hh}^{oa} = A_{op} N_{op} (\varepsilon + \varepsilon_{op})^{1/2} \tag{A2.5}$$

$$P_{hh}^{oe} = A_{op} (N_{op} + 1)(\varepsilon - \varepsilon_{op})^{1/2} \tag{A2.6}$$

$$P_{ll}^{oa} = (m_l/m_h)^{3/2} P_{hh}^{oa} \qquad P_{ll}^{oe} = (m_l/m_h)^{3/2} P_{hh}^{oe}. \tag{A2.7}$$

Inter-sub-band scattering probabilities:

$$P_{hl}^{oa} = P_{ll}^{oa} \qquad P_{hl}^{oe} = P_{ll}^{oe} \qquad P_{lh}^{oa} = P_{hh}^{oa} \qquad P_{lh}^{oe} = P_{hh}^{oe} \tag{A2.8}$$

$$N_{op} = 1/[\exp(\varepsilon_{op}/kT) - 1] \qquad A_{op} = (D_t K)^2 m_h^{3/2}/(\sqrt{2}\pi\hbar^2\rho\varepsilon_{op}). \tag{A2.9}$$

The parameter values are presented in table 1 in paper I.

References

Beregulin E V, Ganichev S D, Glukh K Yu and Yaroshetsky I D 1987 *Fiz. Tekh. Poluprov.* **21** 1005
Beregulin E V, Ganichev S D, Yaroshetsky I D and Yassievich I N 1982 *Fiz. Tekh. Poluprov.* **16** 286
Bishop P J, Gibson A F and Kimmitt M F 1976 *J. Phys. D: Appl. Phys.* **9** L101
Breiland W G, Fayer M D and Harris C B 1976 *Phys. Rev.* A **13** 383
Dargys A 1987 *Phys. Status Solidi* b **143** 675
—— 1989 *J. Phys.: Condens. Matter* **1** 9637
Kane E O 1956 *J. Phys. Chem. Solids* **1** 82
Keilmann F 1977 *Appl. Phys.* **14** 29
Normantas E 1982 *Fiz. Tekh. Poluprov.* **16** 630
Parshin D A and Shabayev A R 1987 *Zh. Eksp. Teor. Fiz.* **92** 1471
Phipps C R and Thomas S J 1977 *Opt. Lett.* **1** 93
Rees H D 1969 *J. Phys. Chem. Solids* **30** 643
Reggiani L, Canali C, Nava F and Ottaviani G 1977 *Phys. Rev.* B **16** 2781
Yuen S Y, Aggarwal R L and Lax B 1980 *J. Appl. Phys.* **51** 1146